# Assessment of the role of micropore size and N-doping in $CO_2$ capture by porous carbons

Marta Sevilla,* Jose B. Parra and Antonio B. Fuertes

*Instituto Nacional del Carbón (CSIC), P.O. Box 73, Oviedo 33080, Spain*

**Keywords:** adsorption, porosity, N-doping, $CO_2$ capture, carbon

## Abstract

The role of micropore size and N-doping in $CO_2$ capture by microporous carbons has been investigated by analyzing the $CO_2$ adsorption properties of two types of activated carbons with analogous textural properties: a) N-free carbon microspheres and b) N-doped carbon microspheres. Both materials exhibit a porosity made up exclusively of micropores ranging in size between < 0.6 nm in the case of the pristine materials and up to 1.6 nm for the highly activated carbons (47 % burn-off). The N-doped carbons possess ~ 3 wt % of N heteroatoms that are incorporated into several types of functional groups (*i. e.* pyrrole/pyridone, pyridine, quaternary and pyridine-N-oxide). Under conventional operation conditions (*i. e.* T ~ 0 – 25 °C and $P_{CO2}$ ~ 0 – 1 bar), $CO_2$ adsorption proceeds via a volume-filling mechanism, the size limit for volume-filling being ~ 0.7 - 0.8 nm. Under these circumstances, the adsorption of $CO_2$ by non-functionalized porous carbons is mainly determined by the volume of the micropores with a size below 0.8 nm. It was also observed that the $CO_2$ capture capacities of un-doped and N-doped carbons are analogous which shows that the nitrogen functionalities present in these N-doped samples do not influence $CO_2$ adsorption. Taking into account the temperature invariance of the characteristic curve postulated by the Dubinin theory, we show that $CO_2$ uptakes can be accurately predicted by using the adsorption data measured at just one temperature.

## Introduction

CO$_2$ capture by means of adsorption in porous materials using pressure and/or temperature swing approaches is receiving increasing attention due to the advantages it offers over conventional technologies based on aqueous amine solvents. These advantages include reduced energy consumption for regeneration, greater capture capacity, ease of handling, reduced environmental impact, etc. A great deal of research effort is therefore being directed towards the design and synthesis of high performance porous sorbents for CO$_2$ capture from flue gas. Such sorbents are superior in terms of capacity, stability, kinetics, selectivity and regeneration. A wide range of sorbents have been analysed, including porous carbons,[1-3] zeolites,[4,5] MOFs[6,7] and microporous polymers.[8,9] Especially, high CO$_2$ adsorption capacities have been achieved with microporous carbon materials.[2,10] Recently, Presser et al. empirically deduced that in the case of microporous carbons, CO$_2$ capture at atmospheric pressure is very much dependent on the number of micropores smaller than 0.8 nm.[1] Following their initiative, Wei et al. and Sevilla et al. found similar results for a variety of activated carbons.[11,12] However, neither of them provides any explanation as to why micropores of this size are important for the adsorption of CO$_2$ molecules.

Some authors have tried to enhance the interaction of porous carbons with CO$_2$ molecules by mimicking the amine scrubbing process (*i.e.* by grafting/impregnating amines or by introducing basic nitrogen functionalities into the porous framework). This last method can be tackled either by (i) carbonizing the N-containing precursor or mixtures of nitrogen-containing organic compounds (i.e. melamine, urea, etc) with N-free materials [13-15] or by (ii) heat-treatment with N-containing gases (i. e. NH$_3$). [16,17] Amine-functionalization has been proved to lead to an enhancement of the isosteric heat of adsorption (40 - 90 kJ/mol), [18-20] yielding values typical of a

chemisorption process, which makes it possible to adsorb at higher temperatures and improve selectivity. However, this is achieved at expense of a drastic drop of the porous properties.[21] This has directed the attention of researchers to the study of N-doping of carbon materials as an alternative method of increasing $CO_2$ capture capacity. Indeed, several authors have suggested that the presence of N heteroatoms in carbonized-activated carbons enhances their performance for $CO_2$ capture.[3,14,22-26] However, to attribute this enhancement solely to N functionalities is impossible due to the fact that other factors, such as micropore size distribution or micropore volume, also play an important role. In fact, most of the works in this area analyse exclusively the performance of N-doped carbons without any reference to un-doped carbons with similar textural properties. Furthermore, the benefits attributed to N-doped carbons with respect to un-doped carbons in relation to $CO_2$ capture are in many cases merely marginal. Therefore, up to date there is no clear evidence about the role that N heteroatoms present in carbonized-activated materials play in $CO_2$ adsorption.

Bearing in mind these ideas, the main objectives of this study are: a) to clarify the effect that the size of micropores has on $CO_2$ adsorption capacity and b) to evaluate the importance of the presence of N heteroatoms for $CO_2$ capture. In order to attain these objectives, we decided to appraise each of these contributions separately by using microporous carbons with similar textural properties but differing in their N-content. To this end, we prepared two activated carbon series: a) five samples with activation degrees in the 0 - 47 % range and b) five samples with similar burn-off degrees but containing around 3 wt % nitrogen. Special care was taken to ensure that for each activation degree, the un-doped and N-doped samples had similar textural properties. In order to determine the role of micropore size, special attention was paid to the fabrication of materials with uniform micropores. The synthesis of such materials was carried out

by physical activation with $CO_2$ as activating agent. To ensure uniform micropore development, the gasification reaction was carried out close to chemical control and diffusional restrictions were minimized. To meet this requirement, we used small porous carbonaceous particles (< 1 micron) as starting material and the reaction with $CO_2$ was carried out at very slow gasification rates (~ 1 - 2 %·h$^{-1}$).

## Results and discussion

### Structural and textural properties of porous carbons

The (resorcinol-formaldehyde)-based carbon consists of uniform colloidal spheres that have a smooth surface and a mean diameter of 0.82 (± 0.06) μm (Figure 1a), whereas the N-doped carbon is formed by interconnected microspheres with a diameter of around 1 micron (Figure 1c). In both cases, after activation, the surface of the particles remains smooth and no roughness is observed. Furthermore, the diameter of the carbon microspheres hardly changes throughout the gasification process, as can be seen from the SEM images of non-activated (Figures 1a and 1c) and activated carbons (burn-off: 35 %) (Figures 1b and 1d). This is corroborated by the size distribution histograms shown in Figure S1 (Supporting Information) for the C-0 and C-3 samples. These results reveal that the mass loss produced as a consequence of the gasification process occurs mainly in the bulk of the carbon particles instead of the surface, which suggests that the gasification reaction proceeds uniformly throughout the carbon particles.
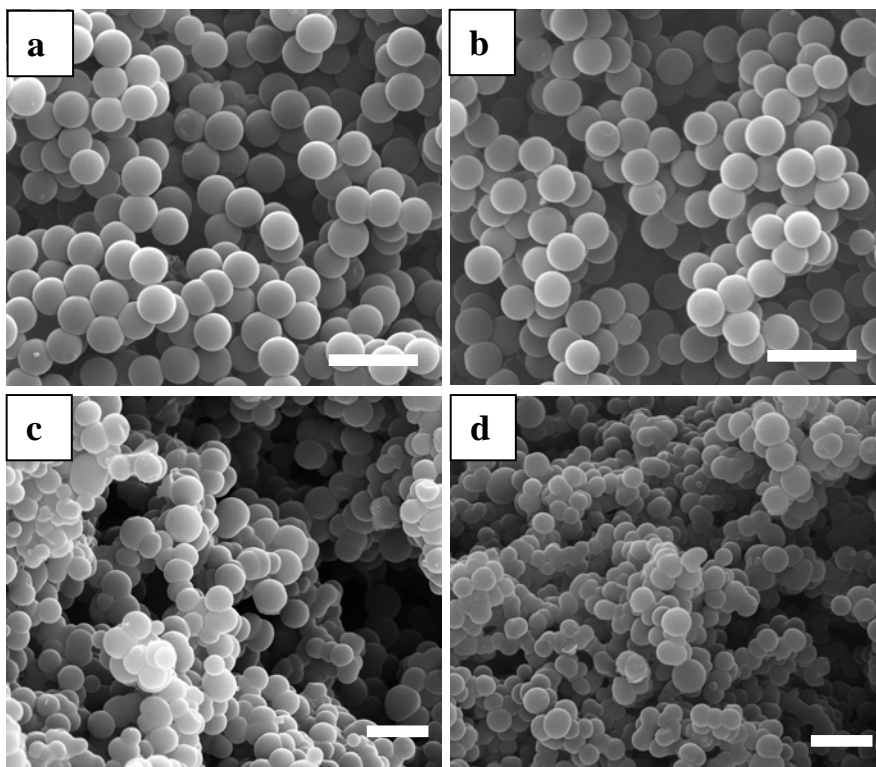
**Figure 1.** SEM images of Stöber-based carbon microspheres (a, b) and N-doped carbon spherules (c, d) of non-activated (a, c) and activated samples at 35 % burn-off (b, d). Bar scale = 2 μm.

The textural properties of the different porous carbons were analyzed by means of gas adsorption of nitrogen at -196 ºC and $CO_2$ at 0 ºC. Figures 2a and 2b compare the nitrogen sorption isotherms for the two series of samples. It can be seen that all the samples exhibit a type I isotherm, which is typical of microporous materials. Moreover, these isotherms exhibit two important characteristics: a) narrow knees at a low relative pressure ($p/p_o$ < 0.03) and b) an absence of adsorption in the pressure range of 0.03-0.9. These results show that the porous carbons have a narrow micropore size distribution and that no mesoporosity is generated during the activation process regardless of the activation degree. In addition, as the activation proceeds, a slight widening of the knee of the isotherms takes place, which suggests an increase in micropore size. This is confirmed by the micropore size distributions (MPSDs) obtained by

means of the QSDFT method (Figures 2c and 2d). These clearly show that a gradual widening of the MPSDs occurs as the activation degree increases. The porosity of the non-activated samples (*i. e.* C-0 and CN-0) is made up almost exclusively of very narrow micropores (< 0.6 nm). As the activation progresses, an enlargement of micropores takes place and, in the case of the medium-activated samples (*i. e.* C-1, C-2, CN-1 and CN-2), a significant fraction of the micropores has sizes in the 0.6 – 1.1 nm range. This is especially evident in the case of the CN samples which exhibit a well-defined maximum of MPSDs at 0.7 - 0.8 nm. Three well-defined micropore ranges can be distinguished for the highly activated samples (*i. e.* C-3, C-4, CN-3 and CN-4): I) very narrow micropores (size < 0.6 nm), II) micropores with sizes in the 0.7 - 0.9 nm range (maximum at ~ 0.8 nm) and III) supermicropores with sizes in the 0.9 - 1.6 nm range (maximum at ~ 1.1 nm), which appear exclusively at high activation degrees.

The textural properties obtained from the analysis of the nitrogen isotherms are shown in Table 1: a) apparent surface area ($S_{BET}$), b) total pore volume ($V_p$), c) micropore surface area ($S_m^t$) and micropore volume ($V_m^t$) deduced by means of the t-plot method. Table 1 also shows the textural properties corresponding to the narrow micropores (*i. e.* micropore volume and average micropore size), which were deduced by applying the Dubinin-Radushkevitch (D-R) equation to the $CO_2$ adsorption data at 0 ºC. The apparent surface areas ($S_{BET}$) regularly increase with the degree of burn-off from 637 $m^2 \cdot g^{-1}$ (C-0) or 510 $m^2 \cdot g^{-1}$ (CN-0) to 1920 $m^2 \cdot g^{-1}$ (C-4) or 1810 $m^2 \cdot g^{-1}$ (CN-4) respectively. They are similar to the microporous surface areas ($S_m^t$) deduced from the t-plot method, which suggests that the porosity of these samples is formed exclusively by micropores. This is confirmed by the fact that the total pore volumes ($V_p$) are quite close to the micropore volume obtained by the t-plot method ($V_m^t$). A comparison of the micropore volumes deduced from the $N_2$ (t-plot, $V_m^t$) and $CO_2$ (D-R plot, $V_o$) adsorption data reveals two interesting

features. In the case of the non-activated samples, $V_o > V_m^t$, reflecting the restriction of the diffusion of $N_2$ molecules in the narrow micropores (< 0.6 nm) (see Figs. 2c and 2d). This is a consequence of the low temperature employed in these experiments. In contrast, for the highly activated carbons (*i. e.* 35 % and 47 % burn-offs) with micropore sizes of up to 1.6 nm (see Figs. 2c and 2d), $V_o < V_m^t$, which is due to the fact that $CO_2$ adsorption is restricted to micropores below 0.8 nm (*vide infra*).

**Table 1**. Textural parameters deduced from the $N_2$ (-196 ºC) and $CO_2$ (0 ºC) adsorption data.

| Sample code | N (wt %) | Burn-off (%) | N₂ adsorption at -196 ºC | | | | CO₂ adsorption at 0 ºC (D-R) | | | | |
|---|---|---|---|---|---|---|---|---|---|---|---|
| | | | | | | | | Micropore system I | | Micropore system II | |
| | | | $S_{BET}$ $(m^2 \cdot g^{-1})$ | $S^t_m$ $(m^2 \cdot g^{-1})$ | $V_p$ $(cm^3 \cdot g^{-1})$ | $V^t_m$ $(cm^3 \cdot g^{-1})$ | $V_o$ $(cm^3 \cdot g^{-1})$ | $V_{o\,I}$ $(cm^3 \cdot g^{-1})$ | $L_I$ (nm) | $V_{o\,II}$ $(cm^3 \cdot g^{-1})$ | $L_{II}$ (nm) |
| C-0 | - | 0 | 640 | 630 | 0.26 | 0.24 | 0.30 | - | - | 0.30 | 0.55 |
| C-1 | - | 15 | 960 | 950 | 0.39 | 0.36 | 0.37 | 0.05 | 0.38 | 0.32 | 0.59 |
| C-2 | - | 24 | 1180 | 1170 | 0.47 | 0.45 | 0.44 | 0.12 | 0.47 | 0.32 | 0.63 |
| C-3 | - | 35 | 1530 | 1520 | 0.62 | 0.59 | 0.52 | 0.22 | 0.57 | 0.30 | 0.74 |
| C-4 | - | 47 | 1920 | 1900 | 0.79 | 0.74 | 0.56 | 0.20 | 0.58 | 0.36 | 0.81 |
| CN-0 | 3.19 | 0 | 510 | 500 | 0.22 | 0.20 | 0.26 | - | - | 0.26 | 0.51 |
| CN-1 | 2.73 | 15 | 900 | 890 | 0.38 | 0.34 | 0.35 | - | - | 0.35 | 0.56 |
| CN-2 | 2.53 | 24 | 1160 | 1130 | 0.48 | 0.43 | 0.39 | 0.08 | 0.42 | 0.31 | 0.61 |
| CN-3 | 3.16 | 35 | 1360 | 1340 | 0.59 | 0.52 | 0.43 | 0.15 | 0.50 | 0.28 | 0.65 |
| CN-4 | 3.13 | 47 | 1810 | 1790 | 0.78 | 0.70 | 0.48 | 0.04 | 0.38 | 0.44 | 0.72 |
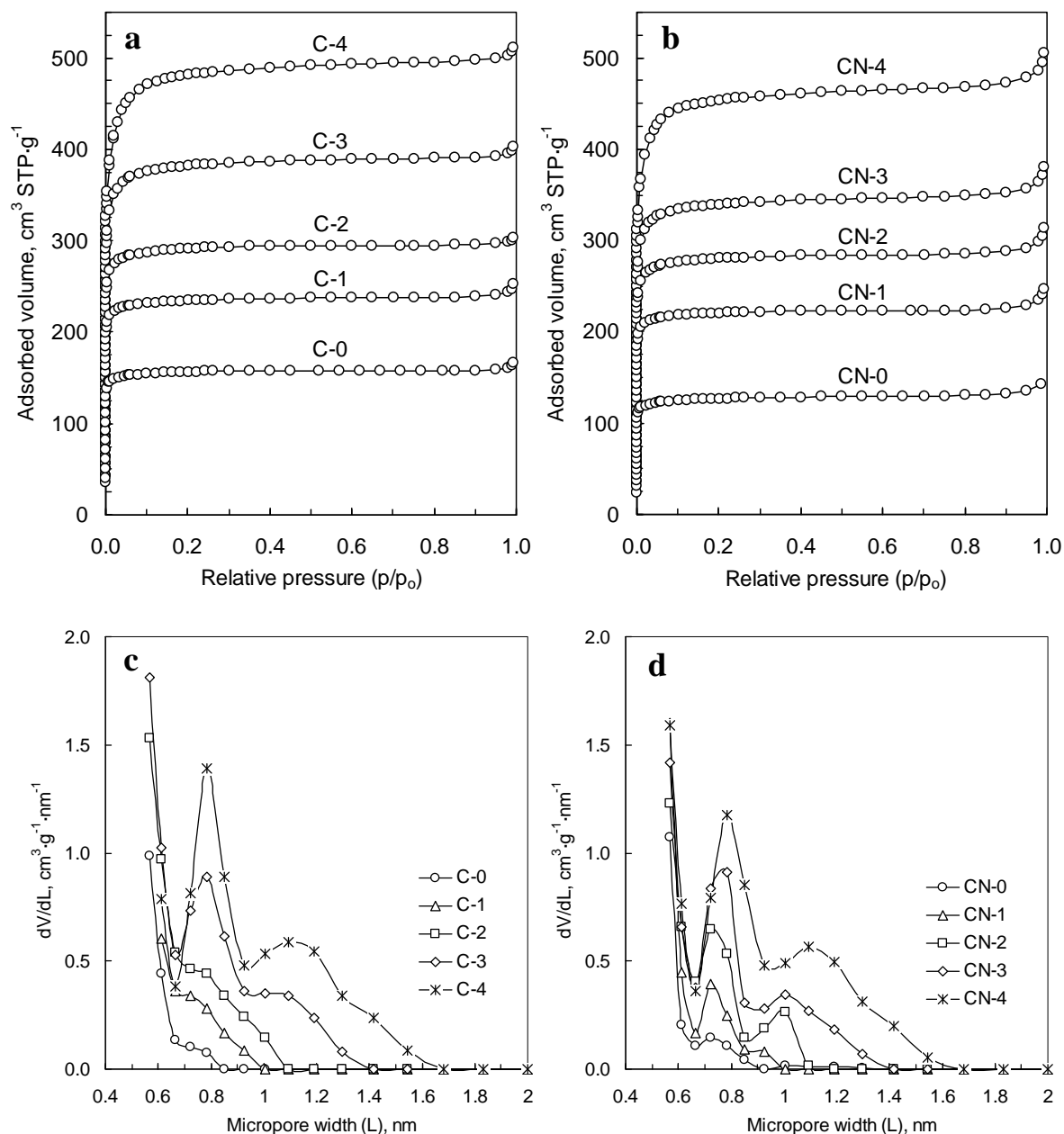
**Figure 2**. Nitrogen sorption isotherms (a, b) and micropore size distributions (c, d) of activated samples.

The $CO_2$ D-R plots provide interesting information about the size of the narrow micropores (< 0.8 nm). Indeed, the slope calculated from the linear form of the D-R equation can be used to estimate the average size of the narrow micropores ($L$), as mentioned in the experimental section. In the case of the non-activated samples, the D-R plot shows a well-defined linear behavior over the entire $A^2$ range (see Figure 3a).

This result shows that the porosity of these samples is made up of uniform micropores, with a size of around 0.5 nm, as deduced from equation (2). It is worth noting that this micropore size is similar to that obtained by the QSDFT method (see Figures 2c and 2d). In contrast, the D-R plots corresponding to the activated samples are non-linear and they exhibit upward deviations at high $A^2$ values, *i. e.* at low relative pressures (see Figure 3b). These deviations appear to be due to the fact that the narrow microporosity is made up of micropores of various sizes. In cases like this, Dubinin et al. postulated the existence of two micropore systems.[27] In this study we adopted this approach and applied it to the $CO_2$ adsorption data of the activated samples, as illustrated in Figure 3b for the C-4 sample. The values of the micropore volume and micropore size corresponding to both pore systems are listed in Table 1. It can be observed that the pore system corresponding to the narrowest pores (System I) is made up of micropores with average widths of around 0.5 nm and that this size hardly changes with the degree of activation. On the other hand, as the activation progresses, a widening of a certain number of micropores (System II) takes place, whose size gradually increases up to ~ 0.7 - 0.8 nm in the case of the samples with 47 % burn-off. ). Again, these results agree with those deduced by the QSDFT method. In fact, micropore systems I and II deduced from the D-R analysis correlate very well with the ranges I and II identified in the MPSDs shown in Figures 2c and 2d. On the other hand, micropore range III (supermicropores with sizes of ~ 0.9 - 1.6 nm) which also appears in these figures, cannot be detected by means of D-R analysis of the $CO_2$ isotherms because under these conditions (0 ºC, 1 bar), the adsorption of this gas is limited to micropores below 0.8 nm (*vide infra*).
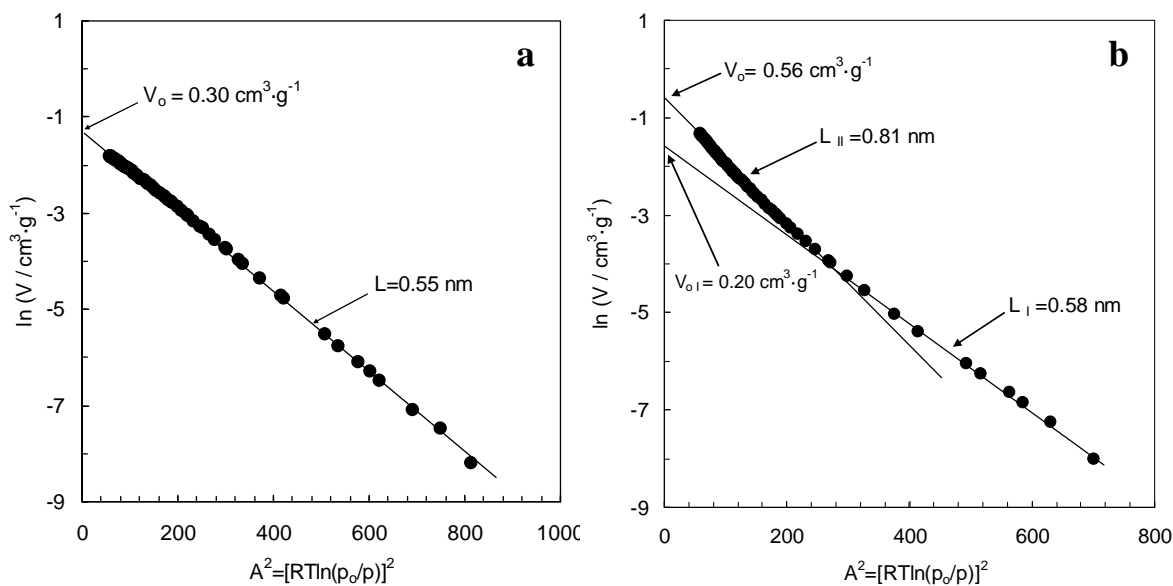
**Figure 3.** D-R plots for the adsorption of $CO_2$ by (a) C-0 and (b) C-4 samples at 0 ºC.

## Relevance of micropore size for $CO_2$ adsorption

For non-polar adsorbate molecules and non-functionalized adsorbent surfaces, the adsorbate-adsorbent interaction energy is derived from short-range attractive and repulsive forces (non-specific interactions).[28] This interaction energy is substantially enhanced when the adsorption takes place in very narrow pores because of the overlapping of the potential fields from the neighboring walls.[29] This enhanced adsorption potential can lead to the complete filling of the narrow micropores at very low relative pressures ($p/p_o < 0.01$). Under these circumstances, the adsorption mechanism consists of volume-filling rather than surface coverage typical of meso-macroporous materials and the adsorbate molecules occupying these narrow micropores are in a liquid-like state.[30] A description of the volume-filling mechanism has been provided by Dubinin, who deduced a relationship between the degree of micropore-filling and the partial pressure of the adsorbate (D-R equation).[31] Theoretical calculations have demonstrated that enhancement of the adsorption energy is negligible for micropore widths larger than around two times (slit-shaped pores) or three times (cylindrical-shaped pores) the molecular diameter.[32] Taking into account that the shape

of micropore in carbonaceous materials is closer to a slit than a cylinder, the size limit for volume-filling can be established at ~ 0.7 - 0.8 nm for $CO_2$ (Kinetic diameter of $CO_2$ ~ 0.33 nm). This result is very important in relation to $CO_2$ capture by carbonaceous adsorbents under conventional operational conditions (temperatures in the 0 - 25 ºC range and $CO_2$ pressures in the 0 - 1 bar range). In fact, under these circumstances, the $CO_2$ relative pressures are very low ($p/p_o < 0.03$) and the adsorption of $CO_2$ occurs via a volume-filling mechanism. Thus, it can be inferred that at these low relative pressures, only those adsorbents with a large number of narrow micropores below ~ 0.8 nm will be able to capture appreciable amounts of $CO_2$. This result clearly suggests that the amount of $CO_2$ captured by non-functionalized porous carbons is mainly determined by the volume of micropores with a size below 0.8 nm. This conclusion is similar to that which was empirically deduced by Presser et al. by correlating the $CO_2$ uptakes and the micropore volumes of a variety of CDCs.[1] Conversely, other pores present in porous carbons such as supermicropores (0.8 - 2 nm) or mesopores (> 2 nm), are not relevant for $CO_2$ capture under conventional operational conditions (i. e. T ~ 0-25 ºC, $p_{CO2} \leq 1$ bar). This is because they are unable to adsorb significant $CO_2$ amounts at the very low relative pressures existing under such conditions. This is the reason for the lack of correlation between the $CO_2$ adsorption capacity of porous carbons and their overall textural properties such as total pore volume or BET surface area. At this point, it is important to mention that when the adsorption is performed up to pressures close to saturation (*i. e.* 35 bar or 64 bar at 0 ºC or 25 ºC respectively), the adsorption of $CO_2$ will occur like that of $N_2$ (-196 ºC) in comparable relative pressure ranges.[33] Under these circumstances, $CO_2$ uptakes can be notably enhanced because supermicropores are now able to adsorb $CO_2$ *via* the coverage adsorption mechanism.

Comparison of the shape of the $CO_2$ isotherms corresponding to the pristine materials and activated carbons clearly evidences the enhanced adsorption potential in the materials with the narrowest pores. This is illustrated in Figure 4, where the $CO_2$ adsorbed at different burn-offs is compared at an adsorption temperature of 0 °C. It can be seen that the fraction of $CO_2$ adsorbed at a given pressure decreases with activation degree. This result clearly suggests a reduction in the adsorption potential as a result of the enlargement of the micropores as the activation progresses. Similar results have been obtained for other adsorption temperatures (see Figure S2 in Supporting Information).
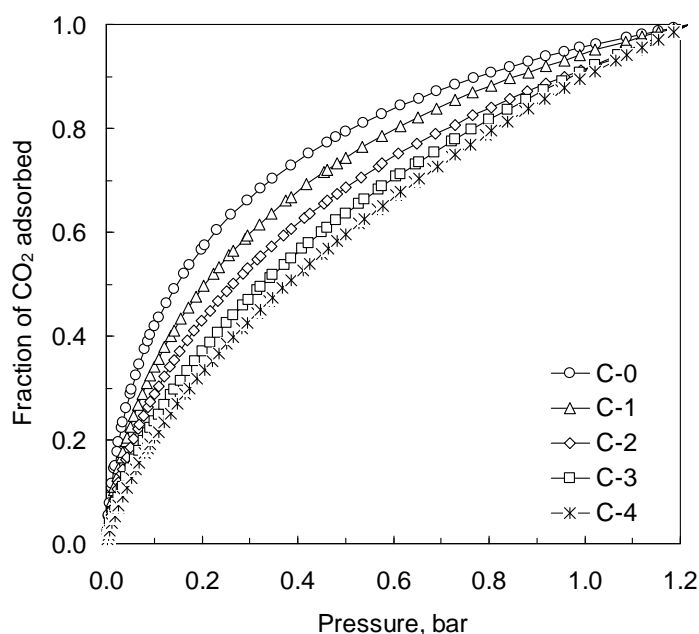


**Figure 4**. Comparison of the fraction of $CO_2$ adsorbed by un-doped carbons at different activation degrees. Adsorption temperature of 0 °C.

An insight into the role of micropores in $CO_2$ adsorption can be obtained by analysing the relationship between the micropore size and the fraction of micropore volume filled by $CO_2$ ($f_{CO2}$). This parameter is defined as $f_{CO2} = q /(V_m \cdot \rho_{CO2})$, where $q$ is the $CO_2$ uptake, $V_m$ is the micropore volume ($V_o$ or $V_m^t$) and $\rho_{CO2}$ is the density of liquid $CO_2$ (1.03 g·cm$^{-3}$ at 0 °C). When the $f_{CO2}$ parameter corresponding to micropores < 0.8

nm (micropore volume = $V_o$) is represented *vs.* the average micropore width $L_{II}$ (Figure 5a), it can be seen that for average micropore widths < 0.65 - 0.7 nm, $f_{CO2}$ remains almost constant, whereas for average micropore widths in the ~ 0.7 - 0.8 nm range, there is a slight decrease in $f_{CO2}$. This result shows that even for average micropore widths of ~ 0.7 - 0.8 nm, there is already a decrease in the enhancement of the adsorption potential. This decrease is even more pronounced if $f_{CO2}$ is determined taking into account the complete range of micropores (micropore volume = $V_m^t$). Thus, as shown in Figure 5b, $f_{CO2}$ steadily decreases with the increase in the average micropore width ($L_o$) deduced by applying the D-R equation to the $N_2$ sorption isotherm. This result is in agreement with the fact that it is micropores below 0.8 nm that are mainly responsible for $CO_2$ adsorption at the low relative pressures used in the experiments carried out under conventional conditions.
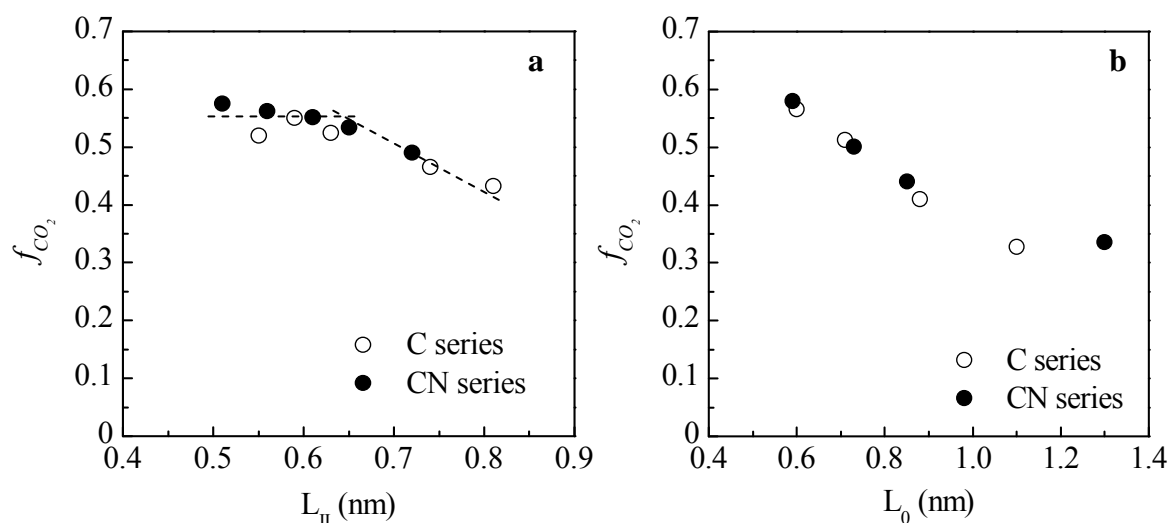


**Figure 5**. Modification of $f_{CO2}$ parameter with average micropore size deduced by applying the D-R plot to the (a) $CO_2$ adsorption (0 ºC) and (b) $N_2$ adsorption (-196 ºC) isotherms.

The variation in $CO_2$ adsorption with temperature might help to clarify the importance of micropore size in this process. In Figure 6a, the modification of $CO_2$ uptakes (measured at 1 bar) with the degree of activation is represented at three

temperatures for both series. It can be seen that, whereas at 25ºC the $CO_2$ uptakes hardly change with burn-off, at – 15 ºC a notable increase occurs. This is due to the fact that at 25 ºC only the narrowest micropores are able to adsorb $CO_2$ because of the low relative pressures ($p/p_o \sim 0.015$ at 25 ºC for $p_{CO2} = 1$ bar). In contrast, at lower adsorption temperatures such as -15 ºC, the $CO_2$ uptake increases substantially with burn-off. This is a consequence of the fact that a certain number of micropores > 0.8 nm are now able to adsorb $CO_2$ owing to the higher relative pressures involved ($p/p_o \sim 0.044$ at -15 ºC for $p_{CO2} = 1$ bar). At this point, it is important to examine the effect of adsorption temperature upon $CO_2$ uptake ($p = 1$ bar). Because adsorption is an exothermic process, in general, $CO_2$ uptake diminishes with temperature. However, the effect of temperature on the quantity of $CO_2$ adsorbed also depends on the pore structure of the adsorbent (*i. e.* pore size distribution). This is evidenced by the results shown in Figure 6b, where the variation in $CO_2$ uptake with temperature is represented for several CN samples by different activation degrees. Interestingly, whereas for the non-activated CN-0 sample (micropores < 0.6 nm), the $CO_2$ uptake diminishes only slightly with temperature, for the highly activated CN-4 sample (micropores up to 1.6 nm) a significant drop is observed. This finding is in accordance with the above results and confirms that the use of sub-zero adsorption temperatures can substantially enhance the $CO_2$ uptakes of highly activated carbons with wide micropore size distributions.
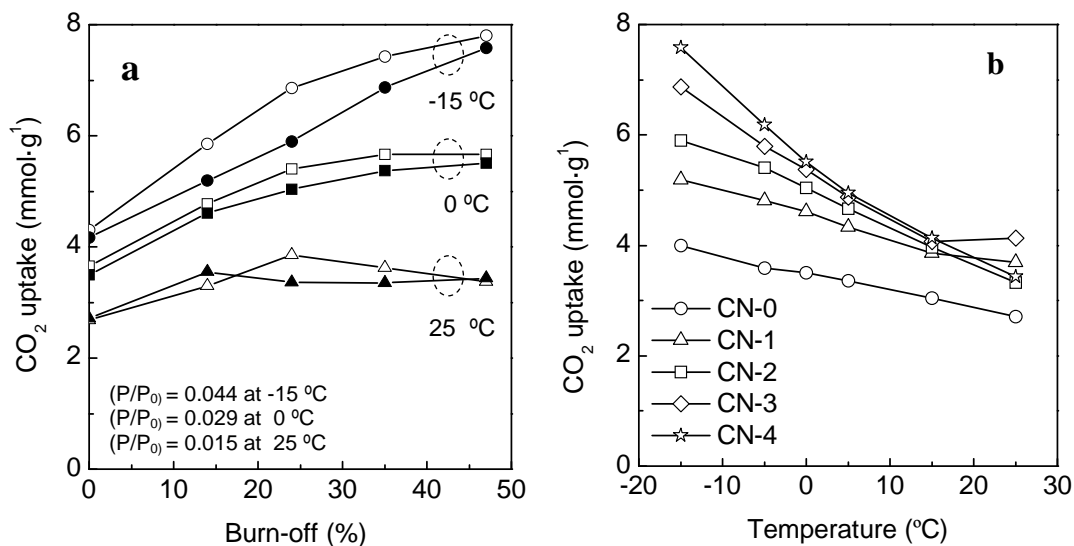
**Figure 6**. Modification of $CO_2$ uptake ($p_{CO2}$=1 bar) with: (a) burn-off for un-doped (open symbols) and N-doped (black symbols) samples, and (b) adsorption temperature for N-doped carbons with different activation degrees.

## Prediction of $CO_2$ adsorption uptakes in activated carbons

It will now be shown that by applying Dubinin's concepts to $CO_2$ adsorption in carbonaceous materials, it is possible to estimate the amounts of $CO_2$ adsorbed at different temperatures by using the adsorption data measured at only one temperature. Indeed, the fundamental postulate of the potential theory is the assumption that the adsorption potential is independent of the temperature and that it exclusively depends on the characteristics of the adsorbent-adsorbate system.[34] This essentially means that, for a given sample, the characteristic curves (*i.e.* V *vs.* RTln($p_o$/p)) should be temperature invariant. The characteristic curves for the C-2 and CN-2 samples at five adsorption temperatures are shown in Figure S3. These curves satisfactorily fulfill the temperature invariance condition. From this it can be inferred that, by measuring $CO_2$ adsorption at a single temperature (usually at 0° C), and calculating the characteristic curve, inverse calculations can be made to obtain isotherms at any other temperature over a range below the critical temperature. In other words, for a particular sample, the

$CO_2$ adsorption data (isotherm) measured at a given temperature will allow the prediction of $CO_2$ uptakes at other temperatures. Figure 7 shows a comparison between the experimental and calculated $CO_2$ uptakes at several temperatures (-15 ºC, -5 ºC, +5 ºC, +15 ºC and +25 ºC) and pressures of 0.2 bar (Fig. 7a), 0.6 bar (Fig. 7b) and 1 bar (Fig. 7c). The $CO_2$ adsorption data measured at 0 ºC for the *C-x* and *CN-x* samples were used as reference. It can be seen that there is an excellent agreement between both sets of data. This result shows that the $CO_2$ uptakes at several temperatures can be accurately predicted by using the adsorption data experimentally measured at a given temperature.
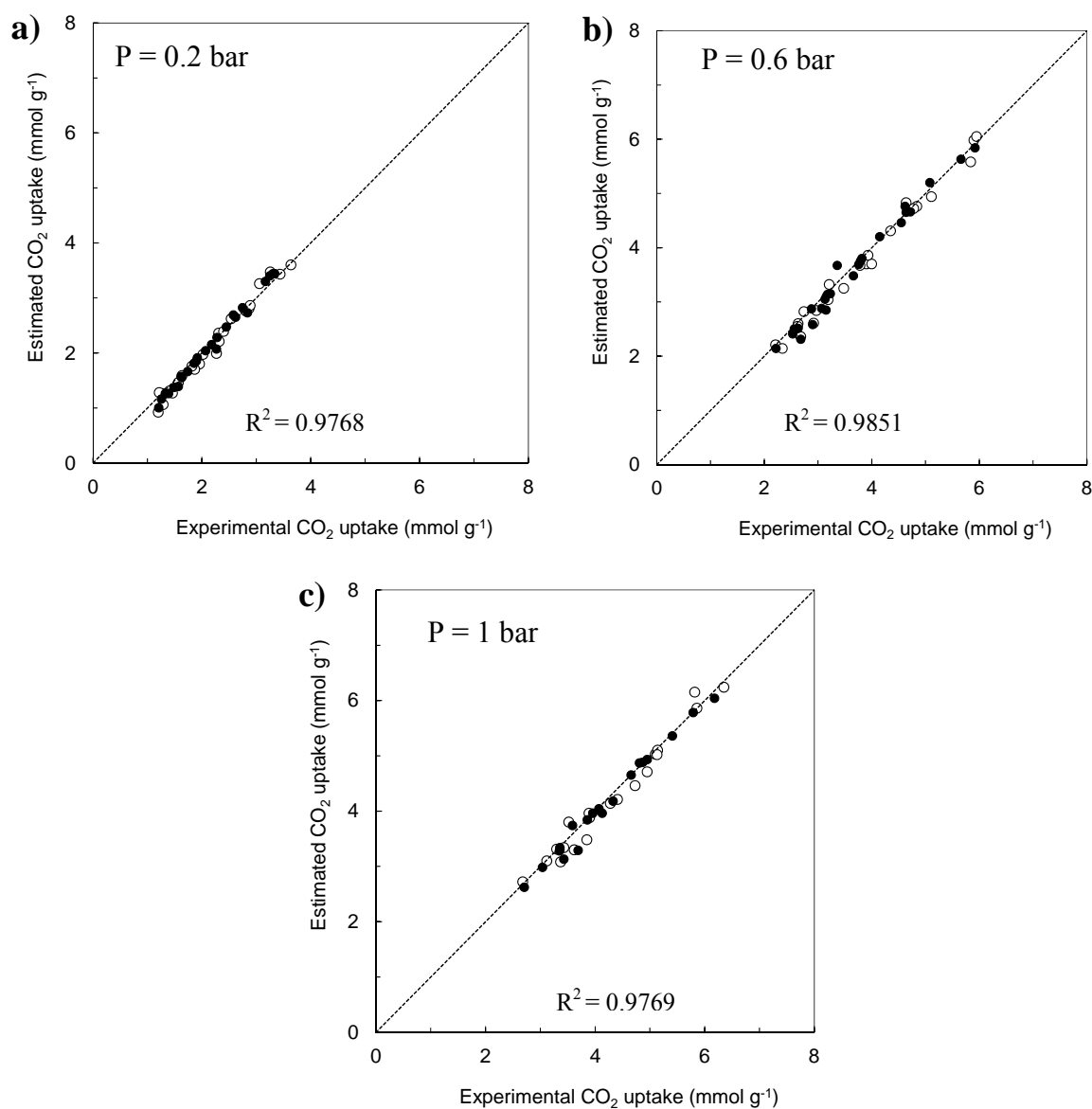
**Figure 7**. Correlation between the experimental $CO_2$ uptakes and those estimated from $CO_2$ adsorption data measured at $0^\circ$ C: (a) 0.2 bar, (b) 0.6 bar and (c) 1 bar. Open symbols refer to un-doped samples and black symbols to N-doped carbons.

**Influence of nitrogen on $CO_2$ capture**

As mentioned in the Introduction section, our strategy for elucidating the role of N heteroatoms in $CO_2$ capture is based on the comparison of the $CO_2$ performance of un-doped and N-doped activated carbons with similar textural properties. The textural data listed in Table 1 reveal that the properties of *C-x* and *CN-x* samples are very similar. It follows that since un-doped and N-doped samples only differ in their N content, a comparison of their $CO_2$ performances will provide information about the role that nitrogen functionalities in the carbonized-activated materials play in $CO_2$ adsorption.

Independently of the activation degree, the *CN-x* samples contain around 3 wt % nitrogen (see Table 1). The nature of the nitrogen functionalities present in the *CN-x* samples was investigated by means of X-ray photoelectron spectroscopy (XPS). Figure S4a illustrates the different kinds of N moieties identified in the analysis of the N 1s core level XPS spectra corresponding to the CN-0 and CN-4 samples (Figure S4b). The following N functional groups were identified: a) pyridinic-N (N-6) at 398.3 eV, b) pyrrole/pyridone (N-5) 400 - 400.4 eV, c) quaternary-N (N-Q) at 401.2 eV and d) pyridine-N-oxide (N-X) at 402.8 eV. Quantitative analysis reveals that the nitrogen in non-activated and activated samples preferentially forms N-6 (~ 40 at. %) and N-Q (24 - 34 at. %) groups, in the order N-6 > N-Q > N-5 > N-X (see Table S1).

To analyse the effect of nitrogen upon $CO_2$ performance, we should envisage two scenarios. In the first scenario the nitrogen heteroatoms present in the carbonized-activated samples are inactive towards $CO_2$ adsorption. Under these circumstances, the amount of $CO_2$ adsorbed will depend exclusively on the adsorption temperature and

textural properties. The second scenario involves the assumption that the N groups have a positive effect on $CO_2$ adsorption and that in consequence a better $CO_2$ performance can be expected for the N-doped than for the un-doped samples with similar textural properties. To elucidate the more probable scenario, we compared the $CO_2$ uptakes measured at a given temperature ($p_{CO2}$=1 bar) for un-doped and N-doped carbons with analogous textural properties (*i. e.* similar activation degrees). The comparison of both sets of data is provided in Figure 8. The results reveal that most of the represented points are below the diagonal line, which suggests that the nitrogen in the N-doped samples does not enhance $CO_2$ performance with respect to the un-doped carbons. What is more, the correlation between these data (dotted line in Fig. 8) reveals that the $CO_2$ uptakes in the case of the un-doped samples are a little better, which is probably because of their slightly better textural properties (see Table 1). On the other hand, Figure 9 compares the adsorption isotherms of C-0/CN-0 (Figure 9a) and C-4/CN-4 (Figure 9b) at three representative temperatures (-15 ºC, 0 ºC and 25 ºC). Remarkably, no significant differences can be appreciated between the isotherms of the un-doped and N-doped samples over the whole pressure range. These results lend strong support to the view that N heteroatoms present in the carbon framework of carbonized-activated carbons do not improve the uptake of $CO_2$. Naturally, this conclusion refers exclusively to carbons with nitrogen functionalities similar to those of the CN samples reported here (*i. e.* N-5, N-6, N-Q and N-X groups). On the other hand, the possibility that the presence of other N-groups (*i. e.* pendant amine groups) enhances the $CO_2$ adsorption capacity of porous carbons cannot be excluded.
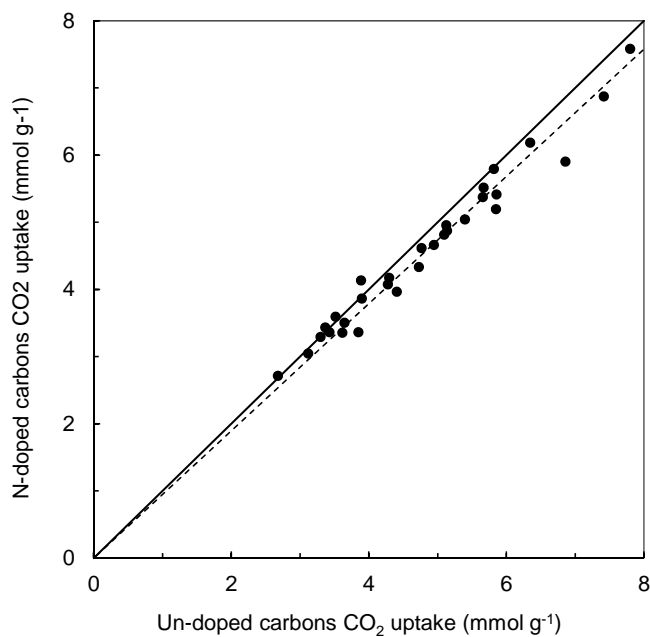
**Figure 8**. Comparison of $CO_2$ uptakes ($p_{CO2}$=1 bar) of un-doped (*x*-axis) and N-doped (*y*-axis) samples. The dashed line shows the fitting of the experimental data (*y=0.95x, $R^2$=0.9632*).
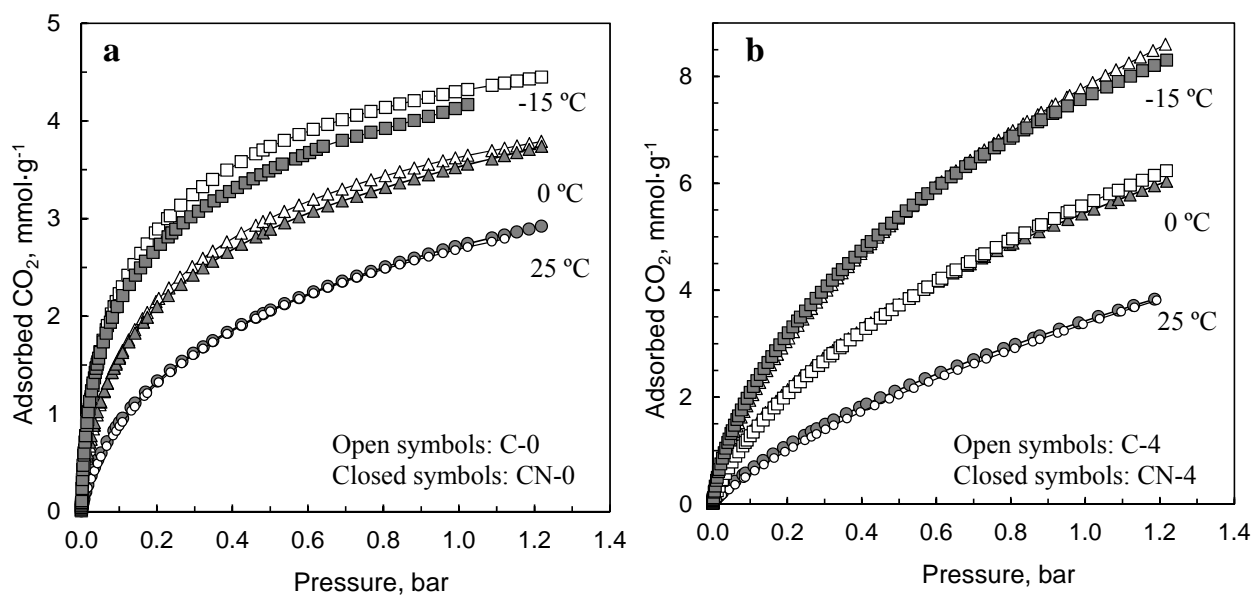


**Figure 9**. Comparison of $CO_2$ isotherms at several temperatures for: (a) non-activated and (b) activated carbons at a burn-off of 47 %.

## Conclusions

N-free and N-doped microporous carbons with analogous textural properties and tunable micropore sizes have been successfully prepared by the physical activation of (resorcinol-formaldehyde)-based carbon microspheres and a N-doped polymeric carbon produced from poly(benzoxazine-co-resol) respectively. Both sets of materials exhibit uniform pore size distributions in the micropore range, this porosity being composed exclusively of narrow micropores (< 0.6 nm) in the case of the pristine materials and micropores of up to 1.6 nm in that of the highly activated samples. The N-doped carbons contain ~ 3 wt % of nitrogen which is incorporated in different functional groups such as pyridinic-N, quaternary-N, pyrrolic-/pyridonic-N and pyridine-N-oxide. The unique textural and chemical properties of these carbon series are the key to evaluating the role of micropore size and N-doping in $CO_2$ adsorption. What is beyond doubt is that $CO_2$ adsorption by microporous carbons depends heavily on micropore size. Thus, under conventional operation conditions (T = 0 – 25 °C and $p_{CO2}$ = 0 – 1 bar), $CO_2$ adsorption in porous carbons takes place *via* a volume-filling mechanism and the micropore size limits for volume-filling are ~ 0.7 - 0.8 nm. Therefore, $CO_2$ adsorption by non-functionalized porous carbons is mainly determined by the volume of micropores with sizes below 0.8 nm. At sub-zero temperatures, supermicropores also contribute to $CO_2$ adsorption because of the increase in relative pressure at these temperatures (*i.e.* $p/p_o$ ~ 0.044 at -15 ºC for $p_{CO2}$ = 1 bar). It follows, therefore, that in the case of highly activated carbons with wide micropore size distributions, $CO_2$ performance can be considerably enhanced by carrying out the adsorption process at sub-zero temperatures. It has also been shown that the nitrogen functionalities present in the microporous carbons analysed in this study do not have any appreciable influence on $CO_2$ adsorption. Finally, we demonstrated that by taking into account the

temperature invariance of the characteristic curve postulated by the Dubinin theory, $CO_2$ uptakes can be accurately predicted on the basis of the adsorption data obtained at just one temperature.

## Experimental section

### Synthesis of porous carbons

*Stöber carbon microspheres.* Resorcinol-formaldehyde microspheres were synthesized according to the procedure reported by Liu et al.[35] Briefly, 1.05 g of ammonia aqueous solution (5 M) was added to 94 g of an ethanol-water mixture (ethanol/water volume ratio = 0.4) and stirred at 30 ºC for 10 minutes. Afterwards, 0.71 g (6.4 mmol) of resorcinol (Aldrich) and 1.1 mL of formalin solution (35 wt % formaldehyde, Aldrich) were added and the reaction mixture was stirred at 30 ºC for 22 h. It was then heated for 24 h at 100 ºC under static conditions in a Teflon autoclave. The solid product was recovered by centrifugation and dried at 100 ºC. Finally, the polymeric microspheres were carbonized under $N_2$ at 800 ºC (5 ºC/min, 1 h).

*N-doped carbon.* A nitrogen-rich polymer (poly(benzoxazine-co-resol)) was used as precursor to synthesize the N-doped carbons. The synthesis procedure is similar to that recently reported by Hao et al.[36] In a typical synthesis, 0.42 g (0.033 mmol) of Pluronic F-127 (Aldrich) and 1 g (9.1 mmol) of resorcinol were dissolved in a mixture of water (3 mL) and ethanol (3.8 mL) under magnetic stirring at room temperature. Afterwards, 0.25 mL (1.32 mmol) of tetraethylenepentamine (Aldrich) was injected into the above solution which was then stirred for 30 min at room temperature. Subsequently, 1.5 mL of formalin solution (18.5 mmol of formaldehyde) was added. The resulting reaction mixture was stirred for ten minutes. The solution was then poured into a Teflon

autoclave which was placed in an oven at 90 ºC and left for 4 h. The resulting polymeric monolith was dried at 50 ºC for 24 h and, then carbonized under $N_2$ at 800 ºC (5 ºC/min, 1 h).

*Physical activation.* In order to increase the porosity, the carbonized materials were activated by using $CO_2$ as gasifying agent. The reaction was carried out in a thermogravimetric system (CI Electronics), which allowed knowing the gasification rate to be followed all the time. In a typical gasification experiment, around 200 mg of carbonized material was employed. In order to ensure a uniform activation, the gasification rates were restricted to ~ 1 - 2 %·h$^{-1}$. The gasification rate was controlled by modifying the reaction temperatures at around 800ºC (±20 ºC). By means of this gasification procedure it was possible to fabricate porous carbons with well-defined activation degrees rising from 15 % to 47 %. The carbons thus produced were denoted as *C-x* or *CN-x* for un-doped or N-doped carbons respectively where *x* was a number that referred to the gasification degree (see Table 1).

**Characterization of materials**

The nitrogen sorption isotherms of the carbon samples were measured at −196 °C using a Micromeritics ASAP 2020 sorptometer, whereas the carbon dioxide isotherms were measured in the -15 – 25 ºC range using a Micromeritics TriStar II sorptometer. The apparent surface area ($S_{BET}$) was calculated from the $N_2$ isotherms using the BET method. An appropriate relative pressure range was selected to ensure that a positive line intersect of multi-point BET fitting *(C > 0)* would be obtained and $V_{ads}(1-p/p_o)$ would increase with $p/p_o$.[30,37] The total pore volume ($V_p$) was determined from the amount of nitrogen adsorbed at a relative pressure ($p/p_o$) of 0.99. The micropore volume ($V_m^t$) and micropore surface area ($S_m^t$) were obtained by applying a *t*-plot analysis (Harkins and Jura thickness equation) to the $N_2$ sorption isotherms. The

micropore size distributions (MPSDs) were determined by means of the Quenched-Solid Density Functional Theory (QSDFT) method applied to the nitrogen adsorption data and assuming a slit pore model.

The $CO_2$ adsorption data obtained at 0 ºC were used to analyze the narrow microporosity by means of the Dubinin–Radushkevich (D-R) equation[38]

$$V = V_o \exp\left[-\left(A/\beta E_o\right)^2\right]$$
(1)

where $V$ is the volume filled at a temperature $T$ and the relative pressure $(p/p_o)$, $V_o$ is the micropore volume, $A = RT \ln (p_o/p)$, and $E_o$ and $\beta$ are the characteristic energy and the affinity coefficient ($\beta$=0.35 for $CO_2$) respectively. The average micropore width, $L$ was calculated by means of the empirical correlation proposed by Stoeckli et al.: [39]

$L (nm) = 10.8 / (E_o\text{-}11.4)$
(2)

Scanning electron microscopy (SEM) images were obtained on a Quanta FEG650 (FEI) instrument. X-ray photoelectron spectroscopy (XPS) was carried out on a Specs spectrometer, using Mg Kα (1253.6 eV) radiation from a double anode at 150 w. Binding energies for the high resolution spectra were calibrated by setting C 1s to 284.6 eV. Elemental analysis (C, H, N) of the samples was carried out on a LECO CHN-932 microanalyzer.

## ASSOCIATED CONTENT

**Supporting Information**

Particle size distributions of pristine and activated materials, comparison of the fraction of $CO_2$ adsorbed at different temperatures for pristine and activated materials, characteristic curves at different temperatures for N-free and N-doped materials, and

XPS results. This material is available free of charge via the Internet at http://pubs.acs.org.

## AUTHOR INFORMATION

**Corresponding author**

martasev@incar.csic.es

**References**

(1)     Presser, V.; McDonough, J.; Yeon, S. H.; Gogotsi, Y. *Energ. Environ. Sci.* **2011**, 4, 3059-3066.
(2)     Sevilla, M.; Fuertes, A. B. *Energ. Environ. Sci.* **2011**, 4, 1765-1771.
(3)     Xia, Y.; Mokaya, R.; Walker, G. S.; Zhu, Y. *Adv. Energy Mater.* **2011**, 1, 678683.
(4)     Siriwardane, R. V.; Shen, M.-S.; Fisher, E. P.; Losch, J. *Energ. Fuel* **2005**, 19, 1153-1159.
(5)     Cavenati, S.; Grande, C. A.; Rodrigues, A. E. *J. Chem. Eng. Data* **2004**, 49, 1095-1101.
(6)     Simmons, J. M.; Wu, H.; Zhou, W.; Yildirim, T. *Energ. Environ. Sci.* **2011**, 4, 2177-2185.
(7)     Bae, Y.-S.; Snurr, R. Q. *Angew. Chem. Int. Ed.* **2011**, 50, 11586-11596.
(8)     Dawson, R.; Stockel, E.; Holst, J. R.; Adams, D. J.; Cooper, A. I. *Energ. Environ. Sci.* **2011**, 4, 4239-4245.
(9)     Lim, H.; Cha, M. C.; Chang, J. Y. *Macromol. Chem. Phys* **2012**, 213, 1385-1390.
(10)    Wahby, A.; Ramos-Fernandez, J. M.; Martinez-Escandell, M.; Sepulveda-Escribano, A.; Silvestre-Albero, J.; Rodriguez-Reinoso, F. *ChemSusChem* **2010**, 3, 974-78.
(11)    Wei, H.; Deng, S.; Hu, B.; Chen, Z.; Wang, B.; Huang, J.; Yu, G. *ChemSusChem* **2012**, 5, 2354- 2360.
(12)    Sevilla, M.; Falco, C.; Titirici, M. M.; Fuertes, A. B. *RSC Advances* **2012**, 2, 12792–12797.

(13)    Liu, R.; Wu, D.; Feng, X.; Müllen, K. *Angew. Chem. Int. Ed.* **2010**, 49, 2565-2569.

(14)    Sevilla, M.; Valle-Vigon, P.; Fuertes, A. B. *Adv. Funct. Mater.* **2011**, 21, 2781-2787.

(15)    Kim, K.-S.; Park, S.-J. *Electrochim. Acta* **2011**, 56, 10130-10137.

(16)    Horikawa, T.; Sakao, N.; Sekida, T.; Hayashi, J. i.; Do, D. D.; Katoh, M. *Carbon* **2012**, 50, 1833-1842.

(17)    Wang, D.-W.; Li, F.; Yin, L.-C.; Lu, X.; Chen, Z.-G.; Gentle, I. R.; Lu, G. Q.; Cheng, H.-M. *Chem. Eur. J.* **2012**, 18, 5345-5351.

(18)    Arstad, B.; Fjellva, H.; Kongshaug, K. O.; Swang, O.; Blom, R. *Adsorption* **2008**, 14, 755-762.

(19)    Bae, Y. S.; Snurr, R. Q. *Angew. Chem. Int. Ed.* **2011**, 50, 11586-11596.

(20)    Mello, M. R.; Phanon, D.; Silveira, G. Q.; Llewellyn, P. L.; Ronconi, C. M. *Microp. Mesop. Mater.* **2011**, 143, 174-179.

(21)    Yue, M. B.; Chun, Y.; Cao, Y.; Dong, X.; Zhu, J. H. *Adv. Funct. Mater.* **2006**, 16, 1717-1722.

(22)    Hao, G.-P.; Li, W.-C.; Qian, D.; Lu, A.-H. *Adv. Mater.* **2010**, 22, 853-857.

(23)    Liu, L.; Deng, Q. F.; Ma, T. Y.; Lin, X. Z.; Hou, X. X.; Liu, Y. P.; Yuan, Z. Y. *J. Mater. Chem.* **2011**, 21, 16001-16009.

(24)    Plaza, M. G.; Rubiera, F.; Pis, J. J.; Pevida, C. *Appl. Surf. Sci.* **2010**, 256, 6843-6849.

(25)    Wang, L.; Yang, R. T. *J. Phys. Chem. C.* **2012**, 116, 1099-1106.

(26)    Zhu, X; Hillesheim, P. C.; Mahurin, S. M.; Wang, C.; Tian, C.; Brown. S.; Luo, H.; Veith, G. M.; Han, K. S.; Hagaman, E. W.; Liu, H.; Dai, S. *ChemSusChem* **2012**, 5, 1912-1917.

(27)    Dubinin, M. M. *Carbon* **1989**, 27, 457-467.

(28)    Gregg, S. J.; Sing, K. S. W. In *Adsorption, surface area and porosity*; Academic Press: London [etc.], **1991**.

(29)    Sing, K. S. W. In *Porosity in carbons: characterization and applications*; J. W. Patrick, Ed; Edward Arnold: London, **1995**; Ch. 2, p 49.

(30)    Rouquerol, F.; Rouquerol, J.; Sing, K. In *Adsorption by powders and porous solids: principles, methodology and applications*; Academic Press: San Diego **1999**.

(31)    Dubinin, M. M. In *Chemistry and Physics of carbon*; P.L. Walker, Jr., Ed.; Marcel Dekker: New York, **1966**; Vol. 2, p 56.

(32)    Everett, D. H.; Powl, J. C. *J. Chem. Soc., Faraday Trans.* **1976**, 72, 619-636.

(33)    Cazorla-Amorós, D.; Alcañiz-Monge, J.; Linares-Solano, A. *Langmuir* **1996**, 12, 2820-2824.

(34)    Dubinin, M. M. *J. Colloid Interf. Sci.* **1967**, 23, 487-499.

(35)    Liu, J.; Qiao, S. Z.; Liu, H.; Chen, J.; Orpe, A.; Zhao, D.; Lu, G. Q. *Angew. Chem.* **2011**, 123, 5894.

(36)    Hao, G.-P.; Li, W.-C.; Qian, D.; Wang, G.-H.; Zhang, W.-P.; Zhang, T.; Wang, A.-Q.; Schüth, F.; Bongard, H.-J.; Lu, A.-H. *J. Am. Chem. Soc.* **2011**, 133, 11378-11388.

(37)    ISO standard 9277:2010. Determination of the specific surface area of solids by gas adsorption - BET method. Second Edition of ISO 9277, ISO, **2012**.

(38)    Dubinin, M. M. *Chem. Rev.* **1960**, 60, 235-241.

(39)    Stoeckli, H. F.; Rebstein, P.; Ballerini, L. *Carbon* **1990**, 28, 907-909.

# TOC

**P: 1 bar / T:-15 to 25 °C**